Thermal and Air Management of an Open Cathode Proton Exchange Membrane Fuel Cell Using Sliding Mode Control

Krishnil Ram, Shanal Kumar, Vincent Léchappé, Ali Mohammadi, Maurizio Cirrincione

Thermal and Air Management of an Open Cathode PEM Fuel Cell using Sliding Mode Control

Krishnil R Ram[1] Shanal S Kumar[1] ,Vincent Léchappé[2], Ali Mohammadi[1], Maurizio Cirrincione[1]

1. *School of Information Technology Engineering Mathematics and Physics, University of the South Pacific ,Suva, Fiji*
2. *Univ Lyon, INSA Lyon, Université Claude Bernard Lyon 1, Ecole Centrale de Lyon, CNRS, Ampère, UMR5505, 69621 Villeurbanne, France.*

Corresponding Author : Krishnil R Ram, Email: ram_k@usp.ac.fj
Postal : School of Information Technology Engineering Mathematics and Physics, University of the South Pacific ,Private Mail Bag, Suva, Fiji.

Keywords: **Fuel Cell , Hydrogen, Oxygen Excess Ratio, Temperature, Sliding Mode Control, Open Cathode**

***Abstract*— The paper presents a simplified nonlinear model for an open cathode Proton Exchange Membrane Fuel Cell (PEMFC) and its control by using three different strategies. The model presented uses four state variables. The mass flow of oxygen, hydrogen flow, water and temperature were taken to be the critical dynamics in the system. The unknown parameters were estimated using the experimental data of a 1.2 kW PEMFC. The simplified model showed good agreement with experimental results. Control schemes were implemented to control the stack temperature of the PEMFC. The Proportional (P) and Proportional Integral (PI) Control performed well but had a poorer response compared to the sliding mode control (SMC) scheme. The study of the different control schemes reveals the dangers of singularly controlling either the oxygen excess ratio or the temperature. Results show the best control is achieved when the excess ratio is control through the reference temperature. The study also compares the parasitic losses from the fans caused by the different controllers. Overall the results provide a good insight into designing a robust control system for an Open Cathode PEMFC for faster response and greater durability.**

I. INTRODUCTION

Fuel Cells offer an emission-free means of energy conversion in stationary power applications as well as in the transport sector. Several types of Fuel Cells such as Solid Oxide Fuel Cells (SOFCs), Direct Methanol Fuel Cells (DMFC) and Polymer Electrolyte Membrane (or Proton Exchange Membrane) (PEM) Fuel Cells dominate the fuel cell market [1]. This paper focuses mainly on PEM Fuel Cells. In general, fuel cells (FC) have an anode and a cathode side. Hydrogen enters through the anode while oxygen enters through the cathode. The reactions of the two gases allow for the generation of electrical energy across the Fuel Cell terminals. With only water and heat as by-products, the PEM Fuel Cell (PEMFC) has no carbon dioxide emission. Open Cathode Fuel Cells do not use supply manifolds fed by compressors and humidifiers hence they have much less patristic losses and have fewer components to maintain. This has made open cathode PEMFC a common choice for low power applications. An open cathode PEMFC has lower costs due to fewer components. The loss of auxiliary equipment requires a better control of the operating parameters for optimal operation. In PEMFC, fans are used to force air through open cathodes to channel the oxygen onto the Membrane Electrode Assembly (MEA). The same air from these fans helps regulate the temperature of the PEMFC. Oxygen is normally obtained from atmospheric air, which is pulled into the PEMFC anode through the axial fans into the open cathode channel. Inside the PEMFC hydrogen and oxygen react with the aid of catalysts to generate electricity. Hydrogen gas is normally controlled through a hydrogen supply valve which functions proportionally to the load current. PEMFC fans must also adjust the flow of oxygen based on the load current. In cases of sudden load increase

the fans must respond quickly and increase the airflow into the system which increases the oxygen flow. If there is less oxygen present that what is required, then two unwanted results take place. Firstly, the desired load will not be met as there would not be sufficient oxygen to react with hydrogen. Secondly, the fuel cell suffers from degradation [2]. For this reason, an excess of oxygen in the cathode is necessary to avoid starvation. Normally Oxygen Excess Ratio (OER) is set at 2 which means twice as much oxygen needs to be supplied than what is being used. The effects of temperature on PEMFC performance is also significant. Several studies have looked at the cell level effects of temperature of fuel cell performance [3], [4] If the temperature is too high, at high pressure the water in the PEMFC will evaporate. The evaporation will lead to dehydration of the membrane. This ultimately reduces membrane conductivity and degrades the cell performance. On the other hand, if the temperature is too low, water retention increases, and the cells get flooded [5] . This slows down the diffusion of gases from the gas diffusion layer (GDL) to the catalyst layer and reduces the performance of the fuel cell. Thus, optimum temperature settings are required in addition to other parameters to ensure efficient water management in the fuel cell [6] . The axial fans that supply air into the cathode also play the role of maintaining stack temperature. Air and Thermal management of the Fuel Cell are critical to avoid fuel cell degradation.

Having an efficient mathematical model greatly aids in developing a robust and fast controller. The models vary in their focus on different dynamics in the PEMFC system. One study [7] presents PEMFC modelling for controlling a large PEMFC with a compressor used to force humidified air into the cathode side. Another researcher [8] has focused on the pressure balance to effectively model the dynamic effects in PEMFC to improve internal designs and external controller designs. PEMFC emulators with dynamic models have also been proposed as a cheap alternative for hardware testing [9]. Detailed models are very useful to observe all the different variables in the system, but these models are difficult to implement and computationally cumbersome. Time delays in PEMFC response arise from the delays in the electrochemical reactions as well. The present work proposes a much-simplified PEMFC model which focuses mainly on the reactant behavior and power output. With the control objective of regulating temperature and excess ratio, the present model is a balance between accuracy and response time of the PEMFC to the demand load profile. Following an accurate and efficient model, a quick responding controller is required. Regarding controlling the temperature and OER of the PEMFC, several works already exist in literature. Several studies have proposed dynamic models and control schemes to control the OER in PEMFC [10], [11]. Classical feedback with Proportional Integral (PI) is one of the most common type of control used in fuel cells performance [12], [13]. The PI or Proportional Integral Differential (PID) control with feedback is generally used to prevent oxygen starvation due to its simplicity and low cost [14], [15]. A multiloop PID control scheme with a multi-objective optimization algorithm was experimentally validated by Gimenez [16]. Zou and Kim proposed a fuzzy control system for a 5kW water cooled PEMFC [17] . Chen et al [10] considered the use of a feedback linearization controller to maintain the OER to an optimum and efficient level. A fractional order based PID controller with unknown input non linear observer was proposed in [18] to maintain the OER in a PEMFC. Another study [19] focused on Active Disturbance Rejection Control (ADRC) and concluded that nonlinear ADRC allowed a better regulation of temperature. Geishernejad [20] utilizes a two step approach by first regulating the input oxygen using a type 2 fuzzy PI (SIT2-FPI) controller then a Deep Deterministic Policy Gradient (DDPG) algorithm is utilized to adjust the PI coefficients of the controller.

The PEMFC and other real life system are prone to several disturbances in operating conditions. One of the controllers that is known to be very robust in the face of disturbances or uncertainties is the Sliding Mode Control (SMC) scheme [21]. Sliding Mode Control is a technique derived from the variable structure control and it was initially studied by Utkin [22]. For incompletely modeled or nonlinear systems it has been proven that Sliding Mode Control is an effective robust control strategy

[23]. Additionally, it has obtained good performance in controlling chemicals processes [24]. Liu et al [25] utilized a disturbance based observer to maintain the OER and maximize power in a PEMFC. Their experimental results showed good transient performances in the presence of load variations and parametric uncertainties. Sankar and Jana [26] studied the SMC control of a reversible PEMFC while incorporating a nonlinear sliding mode based observer . In this study the results of the SMC controller were also compared with a conventional Proportional (P) and PI control schemes. Shanal et al [27] also used a sliding mode controller to maintain the OER with a set reference value of 2 using a very simplified PEMFC model. While most control studies have focused on either the control of OER or the temperature – these two parameters are directly linked in an open cathode PEFC. The fan that provides the flow of oxygen to the cathode also provides the air flowrate for cooling in an Open Cathode PEMFC. This is different from larger systems which are water cooled or air cooled separately while an air compressor provides the required oxygen supply. This study proposes placing the OER in the reference temperature formular in a way that maintains the desired OER and then only the temperature can be controlled while maintaining a minimum OER as well.

II. MATHEMATICAL MODEL

A. Stoichiometry

The stoichiometry of the combined PEMFC reaction yields the molar ratios of reactant gases and products. The chemical reaction in the PEMFC is caused by hydrogen and oxygen gases and produces electricity, heat and water. The reaction is stated as:

$$2H_2 + O_2 \Leftrightarrow 2H_2O$$

From the above reaction, 2 moles of hydrogen gas needs to react with 1 mole of oxygen gas to produce 2 moles of water. If molar masses are considered, then 4 g of hydrogen reacts with 32 g of oxygen gas to form 36 g of water. This gives a hydrogen to oxygen mass ratio of 1:8 for a complete reaction. The current generated during the PEMFC operation is closely linked to the moles of each gas consumed in the reaction: The stack current is given by:

$$I = \frac{m_{O_2} 4F}{M_{O_2}} = \frac{m_{H_2} 2F}{M_{H_2}} \qquad (1)$$

where m_{O_2} and m_{H_2} are the masses of the reactant gases in grams, M_{O_2} and M_{H_2} are the molar masses of oxygen and hydrogen gases, respectively and F is the Faraday constant given in C/mol.

B. Electrical model and voltage losses

Since the reaction takes place across the surface area A_{FC} of the MEA, the current produced is proportional to the area of the MEA or commonly stated as the Fuel Cell area. The current density i is used in determination of voltage losses in the PEMFC and is stated as:

$$i = \frac{I}{A_{FC}} \qquad (2)$$

where A_{FC} is given in [cm$^{2]}$ and the stack current I in [A]. The pressures of hydrogen and oxygen gases are found by using the ideal gas equation. The mass corresponds to the values found by integrating hydrogen and oxygen flow rate equations.

$$p_{O_2} = \frac{m_{O_2} R_{O_2} T}{V_{ca}} \qquad (3)$$

$$p_{H_2} = \frac{m_{H_2} R_{H_2} T}{V_{an}} \qquad (4)$$

Where V_{ca} and V_{an} are the cathode and anode chamber volumes respectively while R_{O_2} and R_{H_2} are the gas constants for the reactants. The Gibbs Free energy equation computes the free energy available for a reversible reaction and allows the system energy to be stated in terms of enthalpy, entropy, and temperature. This reversible electrical potential is the maximum voltage that the fuel cell can produce or the maximum electrical work that can be done. The equation for Gibbs free energy can be given as:

$$W_{electrical} = -\Delta G \quad (5)$$

The Gibbs Free (ΔG) energy value is negative as the energy is given out during the reaction. Gibbs Free energy is calculated at standard state conditions. When there is varying temperature, the Gibbs Free energy is given by [28].

$$W_{electrical} = \Delta G = \Delta H - T\Delta S \quad (6)$$

In this equation ΔH is the change in enthalpy of the system while ΔS is the change in entropy of the system. T is the temperature of the system. The Gibbs Free energy for changing temperature and pressure can be stated as:

$$\Delta G = G_{products} - G_{reactants} = G(H_2O) - G(O_2, H_2) \quad (7)$$

The Gibbs energy value also depends on the state of the water product as some of the energy is involved in a state change. For this reason, if the water (H_2O) product formed in the Fuel Cell reaction is in vapor form – a lower heating value (LHV) of the Gibbs energy is calculated to be 228.6 kJ/mol [29]. The higher heating value (HHV) is found if the water product is in liquid phase. The HHV value is 237 kJ/mol [30]. Since Oxygen and Hydrogen are in their natural elemental state, the Gibbs Free energy is 0 for the reactants. In open cathode Fuel Cells such as the one in this paper, local temperatures and pressures inside the Fuel Cell determine the phase of the water product. The maximum value of Gibbs Free energy in the Fuel Cell is taken as 237 kJ/mol. The maximum electrical potential of the Fuel Cell which is also known as the reversible cell potential E can be found using:

$$E = \frac{\Delta G}{n_e F} \quad (8)$$

In the above equation n_e is the moles of electrons exchanged and F is Faraday's constant. The value of n_e for water formation is taken as 2. Using the HHV of Gibbs Free energy in the above equation, the maximum reversible potential is found to be 1.229 V. The Nernst voltage or the theoretical voltage potential the PEMFC can develop at a certain pressure of hydrogen and oxygen is given by [31].

$$\mathrm{E} = 1.229 - 0.85 \times 10^{-3}(T - 298.15) + 4.3085 \times 10^{-5}\, T \left[\ln(p_{H_2}) + \frac{1}{2}\ln(p_{O_2})\right] \quad (9)$$

While the Nernst voltage provides the theoretical maximum voltage, there are several voltage losses which occur in the PEMFC to reduce the actual output voltage for the cells:

$$v_{fc} = E - (v_{act} + v_{ohm} + v_{conc}) \quad (10)$$

These losses arise from three areas – activation losses, ohmic losses and concentration losses. The activation losses arise due to energy requirements for breaking the bonds and the sluggish rate of reactions at the electrode surface [20].

$$v_{act} = v_0 + v_a(1 - e^{-c_1 i}) \quad (11)$$

where v_a, v_o and c_1 are constants that need to be estimated as shown in [32]. The resistance of electron flow for conducting

electrodes and the resistance of ion flow for the membrane results in ohmic losses:

$$v_{ohm} = i\, R_{ohm} \qquad (12)$$

where R_{ohm} is the internal resistance of the PEMFC. The concentration voltage losses v_{conc} arise due to concentration gradients as the reactants get used up at the cell surfaces and the slow transport of reactants to and from the reaction sites. This can be computed as:

$$v_{conc} = i\left(c_2 \frac{i}{i_{max}}\right)^{c_3} \qquad (13)$$

The reactant flow dynamics in the PEMFC are used in equation 9 to estimate the total theoretical voltage that can be generated by each cell. The reactant gas flow changes in line with the demand current, which can be assumed to be the only input into the system.

$$v_{fc} = 1.229 - 0.85 \times 10^{-3}(T - 298.15) + \ 4.3085 \times \ 10^{-5}\, T\left[\ln(p_{H_2}) + \frac{1}{2}\ln\,(p_{O_2})\right] - (v_{act} + v_{ohm} + v_{conc}) \quad (14)$$

C. Oxygen mass flow

At the cathode, side air is forced into the cathode channels using axial fans. The fans also provide cooling to the PEMFC. The following equation can be obtained by applying the mass conservation at the cathode side, [3]:

$$\dot{m}_{0_2} = \dot{m}_{0_2,in} - \dot{m}_{0_2,used} - \dot{m}_{0_2,out} = \dot{x}_1 \qquad (15)$$

The oxygen mass flowrate considered is the combined oxygen mass flowrate going into the Fuel Cell for both cooling as well as for reaction. The mass of oxygen going into in and out of the FC is not known. Using the mass continuity of oxygen gas allows the problem to be setup in order to determine the mass of oxygen required into the FC. The mass flow rate of oxygen going into the FC is not only a consequence of the gases needed for reaction but also the oxygen excess ratio and requirements of air for cooling. By taking oxygen mass m_{0_2} is a state variable x_1 and noting the load current I_{fc} as the input disturbance to the system (d), then equation 15 can be rewritten as:

$$\dot{m}_{0_2,in} = \lambda_{O_2} y_{o2,ca}\left(1 - \frac{P_{sat}\psi_c}{Kp I_{fc}}\right) Kf I_{fc} \qquad (16)$$

$$\dot{m}_{0_2,used} = \frac{M_{O2} I_{fc} n}{4F} \qquad (17)$$

$$\dot{m}_{0_2,out} = k_{c,out}\dot{m}_{0_2} \qquad (18)$$

$$\dot{x}_1 = \lambda_{O_2} y_{o2,ca}\left(1 - \frac{P_{sat}\psi_c}{k_p I_{fc}}\right) k_f I_{fc} - \frac{M_{O2} I_{fc} n}{4F} - k_{c,out} x_1 \quad (19)$$

Where

$$k_{c,out} = c_4 \qquad (20)$$

$$\frac{M_{O2}\cdot n}{4F} = c_3 \qquad (21)$$

$$y_{o2,ca}\left(\frac{P v_c}{Kp}\right) Kf = c_2 \qquad (22)$$

$$y_{o2,ca}.\, Kf = c_1 \qquad (23)$$

$$\lambda = \frac{\dot{x}_1}{\dot{x}_{ret}} \quad (24)$$

Thus rewriting the equation in terms of reduced parameters:

$$\dot{x}_1(1 + \frac{c_2}{\dot{x}_{\text{ret}}}) = (\lambda c_1 - c_3)u - c_4 x_1 \quad (25)$$

$$\alpha = 1 + \frac{C_2}{x_{\text{ret}}} \quad (26)$$

$$\beta = \lambda c_1 + c_3 \quad (27)$$

Taking the Laplace of the equation gives:

$$(\alpha S_+ c_4)x_1 = \beta u \rightarrow \frac{x_1}{u} = \frac{\beta}{\alpha S + C_4} = \frac{G_0}{\tau S + 1} \quad (29)$$

where λ_{O_2} represents the OER which is generally accepted to be around 2. The molar fraction of oxygen in the incoming air is denoted by $y_{o2,ca}$,while P_{sat} is the saturation pressure of the water at cathode side. The relative humidity is indicated by ψ_c. The inlet side pressure is assumed to be proportional to the input current linearly with the factor k_p as the gradient. The fan conditions are represented as constant k_f. The fan increases its speed based on an increase in load current, and the constants are estimated using characteristic fan curves. Similarly, $k_{c,out}$ represents the effect of the outlet conditions. The constants were estimated empirically by comparing flow rate graphs.

D. Hydrogen mass flow

Similar to the cathode side gas dynamics, the hydrogen gas dynamics can be written by using the net flow of hydrogen where the load current is taken as the input.

$$\dot{x}_2 = \left(1 - \frac{Pv_a}{Pa}\right) k_v I_{fc} - \frac{M_{H2} I_{fc} n}{2F} - k_{a,out} x_2 \quad (30)$$

At the cathode Pv_a is taken as the partial pressure of water vapor while Pa is the pressure of the anode. A valve constant k_v is used to estimate the response of the valve to input current. The outlet flow conditions that affect the mass of hydrogen leaving the anode is taken as $k_{a,out}$.

E. Water mass flow

Most of the water forms at the cathode and this moisture passes through the layers to reach the anode side. The anode water content is essential for this simplified model. It can be assumed that is the water is less compared to the cathode side, and this can be combined directly into the cathode hydration model. The hydration of the membranes also plays an important role in power production and polarization curves.

$$\dot{x}_3 = \frac{m_{H_2O}}{P_{ca}.K_{w1}}.m_{ca} + K_{w2} I_{fc} + \left(K_{w3}.I_{fc} - K_{w4}\right).K_{w5} - \frac{m_{H_2O}}{I_{fc}.K_{w1}.K_{w6}}.m_{ca,out} K_{w7} \quad (31)$$

where K_{w1} , K_{w2}, $K_{w3,}K_{w4}$, K_{w5}, K_{w6} , K_{w7} are constants that have been derived empirically. The flow rate of water is taken as $\dot{x}_3$, m_{ca} is the mass at cathode inlet and $m_{ca.out}$ is the mass at cathode outlet. While the hydration equation is part of the simplified model, it does not affect the control of the OER.

F. Temperature Model

The net heat energy balance of the PEMFC can be simplified to be made up of three quantities. Firstly, there is the heat generated by the chemical reaction which is assumed to be the balance of the higher heating value of hydrogen and the actual electrical voltage generated. This is termed as $\dot{Q}_{GENERATED}$ seen in Fig 1. This heat is a byproduct of the Fuel cell and for an open cathode system, a DC cooling fan may be used to cool the PEMFC by blowing excess air into it. The heat carried away by the cooling fan can be termed as $\dot{Q}_{FAN\ COOLING}$. There is also natural cooling of the PEMFC due to heat loss to surroundings and this can be termed as $\dot{Q}_{NATURAL\ COOLING}$. The heat energy balance can be stated as:

$$\dot{\boldsymbol{Q}}_{\boldsymbol{FC}} = \dot{\boldsymbol{Q}}_{\boldsymbol{GENERATED}} - \dot{\boldsymbol{Q}}_{\boldsymbol{FAN\ COOL}} - \dot{\boldsymbol{Q}}_{\boldsymbol{NATURAL\ COOL}} \quad (32)$$

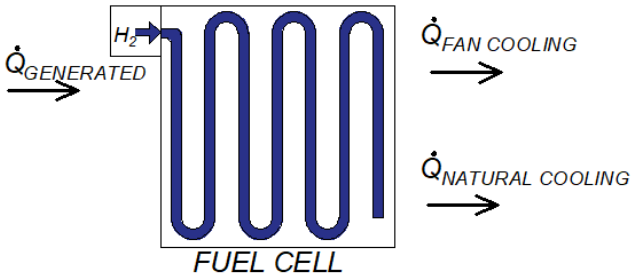

Fig. 1 PEMFC heat flow diagram

While the heat loss to the surrounding is neglected in this paper, the losses are still present in a real system. However, these losses require very careful calculation based on several geometries and materials within the individual Fuel Cell. Additionally, by assuming that there is negligible heat loss to surroundings the fan flow rate ensures that regardless of the heat loss to surrounding –sufficient cooling is provided to maintain the desired temperature in the Fuel Cell. This is an overcompensation and a safety feature as well so that the entire cooling responsibility is that of the fans and there is no reliance on natural cooling. Studies [6], [33], [34]have found that the major contribution to cooling in an open cathode PEMFC is due to forced convection of air from the axial fans. Given that heat loss to surroundings will vary according to environmental conditions and likely be much smaller than forced fan cooling, it can be neglected to form:

$$\dot{Q}_{FC} = \dot{Q}_{GENERATED} - \dot{Q}_{FAN\ COOL} \quad (33)$$

It can be assumed safely that any energy that is not converted to electrical voltage per cell is converted to heat energy.

$$\dot{Q}_{GENERATED} = I_{FC,net}.(1.229n - v_{FC}) \quad (34)$$

The DC fan used to cool the PEMFC will need a mass flow rate of air $\dot{m}_{air}$ to cool the cell from a higher temperature of T to the set reference temperature T_{ref} :

$$\dot{Q}_{FAN\ COOL} = \dot{m}_{air}.C_{p,air}(T - T_{ref}) \quad (35)$$

Dividing by the mass of the PEMFC and its specific heating capacity, the following equations can be found for the temperature:

$$\frac{d_{T_{FC}}}{d_t} = \frac{1}{\dot{m}_{FC}C_{p,FC}}\left[I_{FC,net}.(1.26.n - v_{FC}) - \dot{m}_{air}C_{p_{air}}(T - T_{ref})\right] \quad (36)$$

$$\dot{x}_4 = \frac{1}{K_{fc}}\left[(35.28 - v_{fc})I_{fc} - C_{p_{\text{air}}}\dot{m}_{air}(x_4 - T_{\text{ref}})\right] \quad (37)$$

The fuel cell temperature is considered as $\dot{x}_4$. In the following sections the control schemes are explained in detail.

G. OER control

Two different control topologies are tested on the simplified model to control the OER. The primary control objective is to ensure that the OER is maintained at 2. Firstly, a PI like control scheme is applied as shown in Fig 2: Choosing current as the input for the system u .

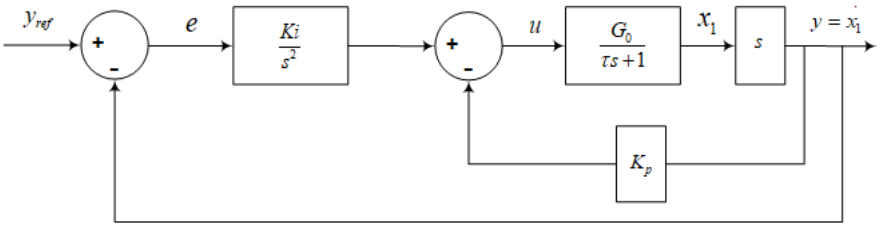

Fig. 2 PI-like Controller scheme for maintaining OER.

where $G_o = 3.65e^{-4}$ and $\tau = 100$ are obtained from equations (19 - 29). From the block diagram of Fig 2, the following equation is derived:

$$\frac{y}{y_{ref}} = \frac{2}{\frac{\tau+K_pG_o}{K_iG_o}s^2+\frac{1}{K_iG_o}s+1} = \frac{2}{\frac{1}{\omega_{CL}^2}s^2+\frac{2\varepsilon_{CL}}{\omega_{CL}}s+1} \quad (38)$$

This transfer function has a gain equal to 2, so the OER $\frac{\dot{x_1}}{\dot{x}_{1ref}} = \lambda_{O_2}$ will be equal to 2. In addition, the closed loop dynamics can be tuned by choosing proper gains K_p and K_i. For desired closed specifications ω_{CL} and ε_{CL}:

$$Ki = \frac{\omega_{CL}}{2G_o\varepsilon_{CL}} \quad (39)$$

$$K_p = \frac{1}{G_o}\left(\frac{K_iG_o}{\omega_{CL}^2} - \tau\right) \quad (40)$$

Taking ε_{CL} = 1 and ω_{CL}= 0.1 gives Ki = 13.6054 and K_p= −1.3605 x 10^5. Given that the system model has been simplified, a robust control strategy needs to be adopted to ensure optimum control despite losing some details in the model. For this reason, a sliding mode control scheme is applied and then compared with a PI control.

The sliding model control equations can be derived from the state equations. Solving for all constants thus:

$$u = \frac{1}{\lambda_{O_2} c1 - c3}(\lambda_{O_2} c_2 + x_1 + v) \quad (41)$$

is obtained from equation (19). The first order sliding mode control topology was developed with the objective of controlling the OER. The following auxiliary control equation can be stated as:

$$v = k_1 y + k_2 y_{ref} + \dot{y} + k_3 sign(e) \quad (42)$$

where k_1 , k_2 and k_3 are gains that were tuned using a Lyapunov analysis. Defining the Lyapunov function candidate as:

$$V = \frac{1}{2} e^2 \quad (43)$$

where $e = y_{ref} - y$ is the sliding surface and taking its time derivative gives:

$$\dot{V} = \dot{e}e$$

$$\dot{V} = -\dot{y}e$$

$$\dot{V} = [(1 - k_1)y - k_2 y_{ref} - k_3 sign(e)]e \quad (44)$$

In particular choosing $k_2 = 1 - k_1$ leads to:

$$\dot{V} = (1 - k_1)e^2 - k_3 sign(e)e \quad (45)$$

Setting $k_1 > 1$, the following inequality can be obtained

$$\dot{V} \leq -k_3\sqrt{2}\sqrt{V} \quad (46)$$

by which V will reach zero in finite time or that y will reach y_{ref} in finite time. The block diagram of the control scheme is shown in Fig. 3.

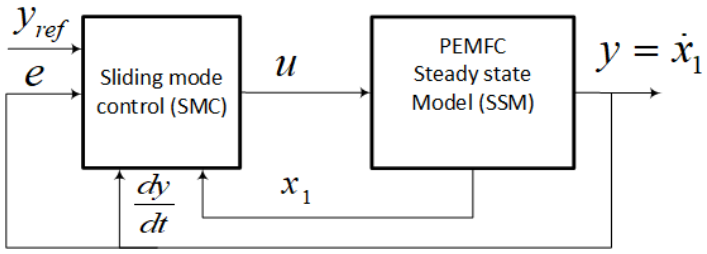

Fig. 3 Sliding Mode Control scheme for maintaining OER.

H. Temperature control design

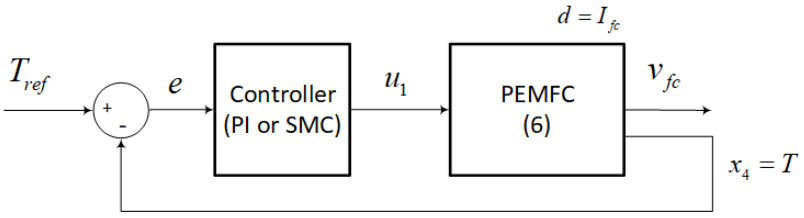

Fig. 4 Temperature Control scheme.

Three different control topologies have been performed for temperature control as shown in Fig. 4. Firstly, the most basic approach of proportional control scheme was applied. Choosing m_{air} as the control input (u_1) for temperature control as shown in the following equation.

$$u_1 = \frac{1}{C_{p_{air}}(x_4 - T_r)}\left[(35.28 - v_{fc})u_1 + k_6 K_{fc}(x_4 - x_{4r})\right] \quad (47)$$

implies

$$\dot{x}_4 = -k_6(x_4 - x_{4r}) \quad (48)$$

Defining $e_6 = x_4 - x_{4r}$ with x_{4r} constant then $\dot{e}_6 = -k_6 e_6$. if $k_6 > 0$ then e_6 tends to 0. Taking the Laplace transform, one gets

$$sx_4 = -k_6 x_4 + k_6 x_{4r} \quad (49)$$

So

$$\frac{x_4(s)}{x_{4r_{6r}}(s)} = \frac{1}{\frac{1}{k_6}s+1} = \frac{1}{\tau_m s+1} \quad (50)$$

With $\tau_m = 1/k_6$. As a result $k_6 = \frac{1}{\tau_m}$ where τ_m can be selected in order to achieve the desired time response of the system.

Second approach was taken as proportional integral controller for temperature.

$$u_1 = \frac{1}{C_{p_{air}}(x_4 - T_r)}\left[(35.28 - v_{fc})I_{fc} + k_6 K_{fc} x_4 + k_7 K_{fc}\int_0^t (x_4(s) - x_{4r})ds\right] \quad (51)$$

implies

$$\dot{x}_4 = -k_6 x_4 - k_7\int_0^t (x_4(s) - x_{4r})ds \quad (52)$$

So by taking the Laplace transform (considering 0 initial conditions):

$$sX_4 = -k_6 \mathrm{X}_4 - \frac{k_7}{s}X_4 + \frac{k_7}{s}x_{4r} \quad (53)$$

$$\frac{x_4(s)}{x_{4r}(s)} = \frac{1}{\frac{1}{k_7}s^2 + \frac{k_6}{k_7}s + 1} = \frac{1}{\frac{1}{\omega_n^2}s^2 + \frac{2\xi}{\omega_n}s + 1} \quad (54)$$

With $\omega_n = \sqrt{k_7}$ and $\xi = \frac{1}{2}\frac{k_6}{\sqrt{k7}}$. If we fix $\xi = 1$ to have a response with no overshoot then $T_{r5\%}\omega_n = 4.74$ so we can compute $\omega_n = 4.74/T_{r5\%}$ where $T_{r5\%}$ is the desired response time and finally

$$k_7 = \omega_n^2$$
$$k_6 = 2\xi\omega_n$$

Finally, the first order sliding mode control scheme was applied in order to control the temperature.

$$u_1 = \frac{1}{C_{p_{air}}(x_4 - T_{\max})}\left[(35.28 - v_{fc})I_{fc} + k_6 K_{fc}\text{sign}\,(x_4 - x_{4r})\right] \quad (55)$$

implies

$$\dot{x}_4 = -k_6\text{sign}\,(x_4 - x_{4r}) \quad (56)$$

The parameters for this model were estimated empirically and from standard data sheets and fluid properties. Other values such as temperature reflect the standard environment conditions. These values are given in Table 1. The parameters for this model were estimated empirically and from standard data sheets and fluid properties.

TABLE I CONSTANTS USED IN THE MODEL

$y_{O_2,ca} = 0.21$	$\lambda_{O_2} = 2$
$P_{sat} = 3.16469\ kPa$	$n = 28$
$N_{max} = 6000\ rpm$	$F = 96{,}485$
$kp = 21kPa$	$k_{c,out} = 0.01$
$Pa = 600\ kPa$	$k_{a,out} = 1 \times 10^{-11}$
$Kf_c = 921$	$\emptyset_a = 1 \times 10^{-4}$
$Kv = 4.2 \times 10^{-7}$	$\psi_c = 0.7$
$M_{H_2} = 2.016\ g/mol$	$M_{O_2} = 32\ g/mol$
$T_r = 298$	$L_m(H) = 25 \times 10^{-6}$
$K_a = 1160$	$g_1 = 0.000377$
$R_m\,(\Omega) = 0.35$	$C_{P_{air}} = 1000$
$Pv_a = \emptyset_a P_{sat}$ $= 3.16510^{-4} kPa$	

III. EXPERIMENTAL SETUP

A 1.2 kW open cathode PEMFC was loaded using a DC electronic load, as shown in Fig. 5. Data was collected from the PEMFC user interface module. A single ramp current load was programmed into the electronic load, starting at 2A and ending at 60A. The PEMFC was not able to output a current lower than 2A. Voltage and current was logged in the electronic load as well. The sampling rate in both cases are 2Hz.

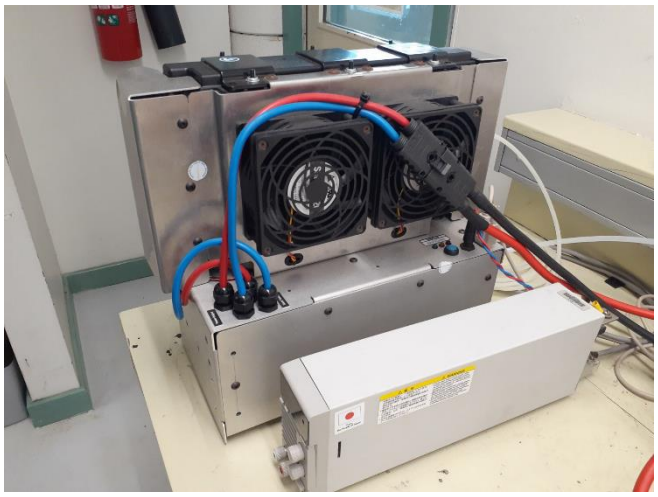

Fig. 5 The 1.2kW Fuel Cell setup.

IV. MODEL RESULTS AND VALIDATION

Simulink model was run for 100s and the resulting polarization curve was compared to the measured experimental data. The PEMFC used to gather the experimental results had 28 cells with a maximum voltage reaching 0.9 V in each cell. The PEMFC area was 62 cm^2 while its membrane thickness was 0.42mm. Parameter estimation was carried out using nonlinear least squares method. The parameter estimation details are stated in [32].

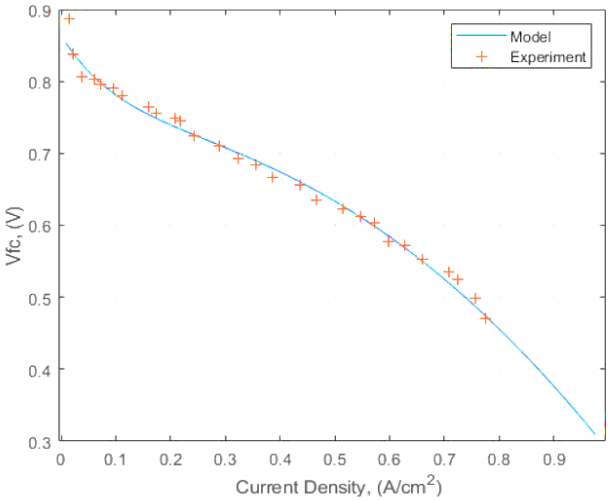

Fig. 6 Experimental and model results compared on Polarization Curve.

Generally, there is good agreement between the polarization curve estimated through the model and the results obtained through experiments as seen in Fig. 6. It is essential for a good PEMFC model to accurately predict the flow rate of gasses for changing load currents. A load profile was applied to the model and the change in flow rates of oxygen and hydrogen are shown in Fig. 7. Given that there is no controller at this stage of the model the reducing flowrate is seen in the model as the load changes.

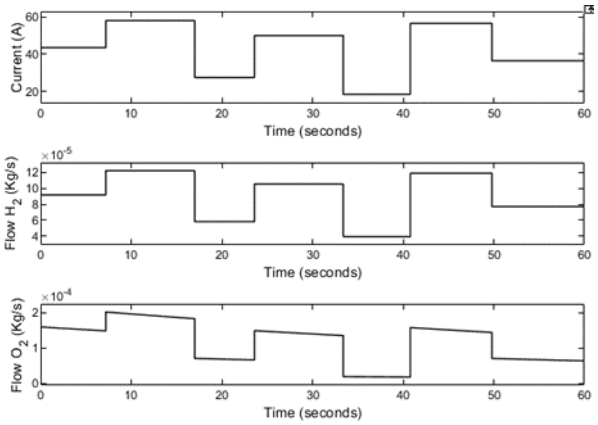

Fig. 7 Reactant gas flow rate variation with respect to load current.

A. Control of Excess Ratio Only

The following results are based on the work done in [27]. For that study the control objective was simply to control the OER to avoid oxygen starvation and degradation of the fuel cell. In the later sections, an improved control scheme is presented which not only controls the excess ratio but the fuel cell temperature as well. There is some delay in flow rate of hydrogen in the system when the load current changes abruptly. For oxygen the delays in following the load current is very high during load changes and even at constant current intervals – the flowrate is poorly maintained. The poor response of oxygen flow without a controller will not achieve the desired stoichiometry and results in power loss. Fig. 8 shows how the OER changes with time. It is noteworthy that between 30s and 40s the excess ratio drops below 1. An excess ratio below 1 means that less oxygen is supplied than what is required to produce the load current. Not only does this result in power loss, but it also causes cell degradation. The results also points towards the need of a controller in the model to accurately represent the functions of a real fuel cell.

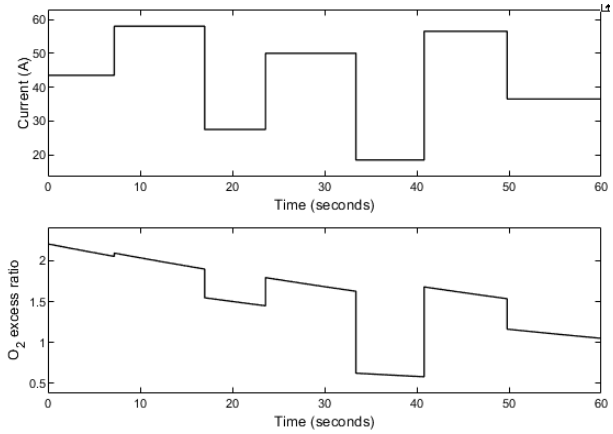

Fig. 8 OER without controller

For the PI controller the gains were tuned to be $K_p = -1.3605e5$ and $Ki = 13.6054$. The use of a PI controller improves the systems OER and oxygen flow response. The results in Fig. 9 clearly show the excess ratio stabilizes around the designed excess ratio of 2, but the response to any change in load current is still inadequate.

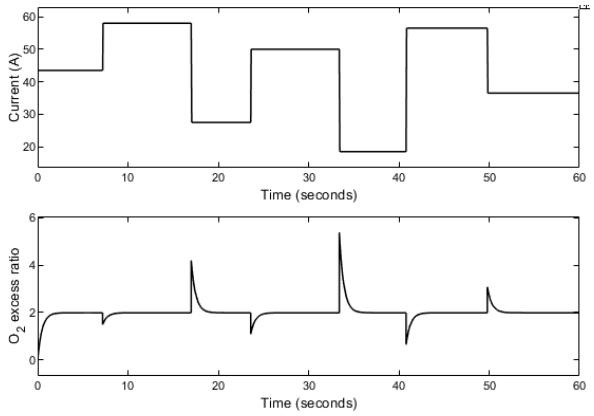

Fig. 9 OER using PI controller.

The response of oxygen flow rate to change in load current is relatively slow and takes almost 1.5s to stabilize. Furthermore, at around 40s when the load changes to 55 A, the excess ratio is seen to drop below one which is unacceptable. This would mean the PEMFC is starved of oxygen.

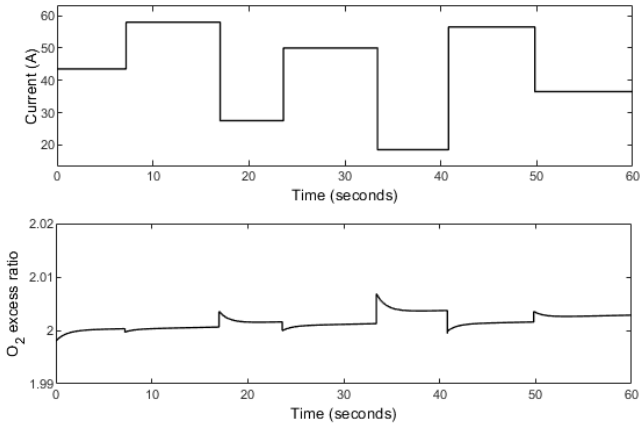

Fig. 10 OER controlled using SMC.

For the SMC the gains were calculated as: $K_1 = 2000$, $K_2 = -1999$ and $K_3 = 1e^{-7}$. The results of the SMC with the objective of maintaining an OER of 2 is shown in Fig 10. It can be seen that the excess ratio is reasonably maintained at around 2 with perturbations of far less than 0.01 from the reference. This is different from the excess ratio maintained by the PI controller where values below 1 were seen. This control topology, therefore, achieves the objective even on a simplified PEMFC model. The oxygen flow rate response is slower when using the traditional PI control with feedback, as shown in Fig 11. This is one of the reasons why the OER is difficult to maintain using a simple PI controller. In an actual system, more delays are anticipated as the oxygen is supplied using an axial fan. Unlike large compressor driven systems, there is no storage of air in a supply manifold, and hence the response of the oxygen supply subsystem is much more critical. In Fig 11 where both the controllers are compared on the same scale, it can be clearly seen that the SMC is able to maintain OER of 2 for the system with an error margin of less than 0.01.

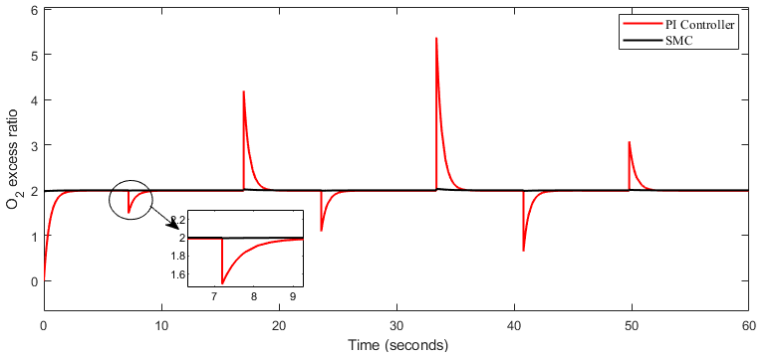

Fig. 11 Magnified view showing the PI response time.

Given the simplified model of the PEMFC, greater emphasis needs to be placed on the controller to account for the loss of details in model simplification. The results so far have only looked at controlling the OER while neglecting the temperature of the PEMFC.

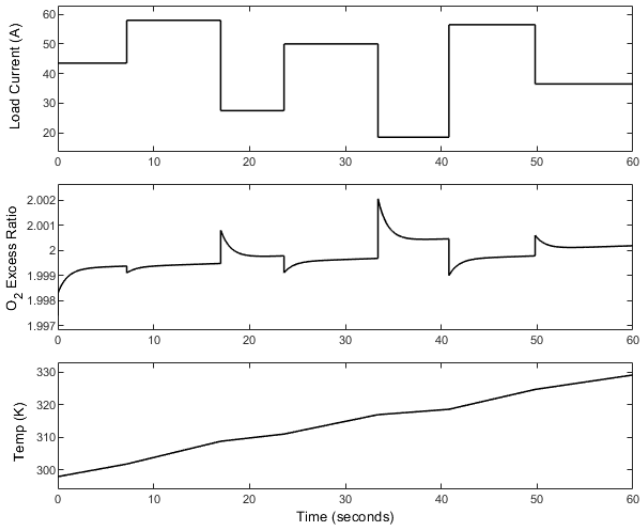

Fig. 12 Comparison of OER with temperature behavior

In Fig. 12, the SMC controller is able to control the excess ratio to stay above a value of 2 (with deviations of less than 0.01 from the setpoint) . However, this excess ratio flow is not sufficient to generate the flowrate to keep the PEMFC cool within the desired temperature range. The PEMFC temperature is seen to rise proportionally with time of use as there is no way to cool the system. This is a likely outcome if only the OER is the focus of the control scheme and will lead to overheating and degradation of the PEMFC.

K. Temperature Control Only

The Temperature can be controlled by setting a reference temperature for optimum performance. For this study the reference temperature values for different load current in this case was derived from experimental and empirical results. The simulation period was also extended for 2000 seconds for this study to be able to understand the changes in temperature which may not be apparent in a shorter period.

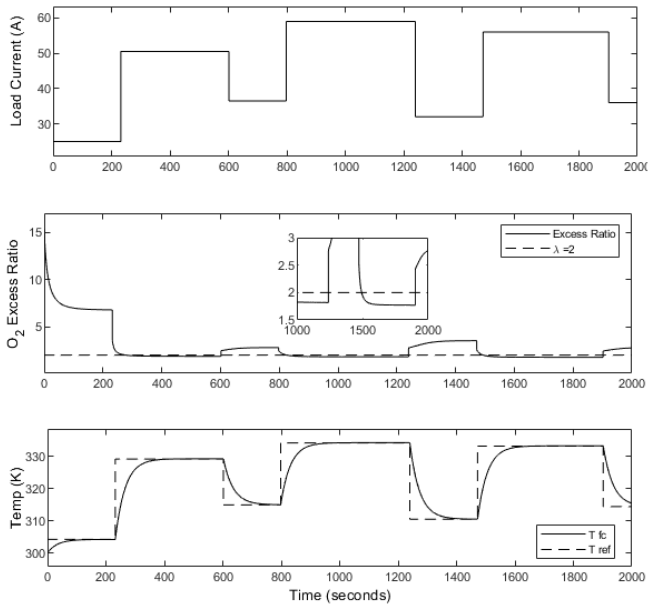

Fig. 13 Comparison of OER with temperature control only using a PI control scheme.

In Fig. 13 the results of controlling the temperature using a PI control scheme is shown. The results show that temperature is controlled well apart from an inherent slow response time. However, it can be noticed that the OER drops to below the desired level of 2. This normally happens in low load situations when the temperature is also low and the fans are not required to actively cool the PEMFC. Also, during sudden load changes, the fans are not able to maintain the excess ratio at a safe level as the temperature rises slowly. Ideally the excess ratio and the temperature both need to be controlled together. In the next section the temperature is controlled by factoring in the excess ratio to set the reference temperatures. Similar results were seen from other controllers that were tested.

L. Control of Temperature with excess ratio

In this case, the control objective is to regulate the temperature based on the input load profile while trying to keep the OER above 2. For and Open Cathode PEMFC, the same fans that supply oxygen rich air for the electrochemical reaction are also responsible for cooling the stack. For this reason, the reference temperature is set using the following equation:

$$Tref = \begin{bmatrix} T_{ref} = \frac{0.9 I_{fc}(1.26n - v_{fc})}{1000\, m_{req}} + T_{room} & ,\lambda < 2 \\ Tref & ,\lambda \geq 2 \end{bmatrix} \qquad (42)$$

Having the OER as a parameter in setting the reference temperature also avoids multiple control loops. Since the reference temperature $Tref$ is proportional and calculated from the load current, as the load changes the reference temperature is checked. A quick check is made to determine the OER based on the $Tref$ and if the OER is found to be below 2, a new reference is calculated which factors in the m_{req} which is the mass of oxygen required to keep the OER at 2 or above. Since the new reference calculation needs to increase the flow rate of oxygen and consequently air – the temperature is slightly lower than the original reference. The drop in the new reference temperature was a few degrees only. As this normally occurs at rising high current loads, the temperature will already be high enough to ensure membrane hydration is not affected even with a slight drop in reference temperature. For this case the P, PI and SMC controllers are compared using the same load current used in the previous section.

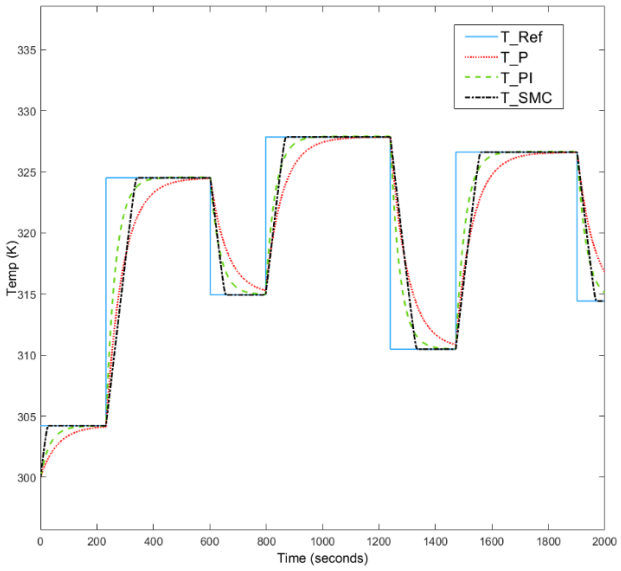

Fig. 14 Temperature reference and outputs from all 3 controllers.

Fig. 14 shows the stack temperature as a response from all 3 controllers . The solid blue line represents the fuel cell stack reference temperature and the dashed red line represents the controlled output from the Proportional controller. The controller is able to maintain the required stack temperature, however, the settling time is around 200 – 250 seconds. This high settling time causes a large delay in achieving the desired stack temperature. The PI controller output is represented by the green dashed line. The PI controller has lower settling times of around 175 seconds. Even with the low settling time, the PI controller's delay in reaching the reference temperatures is not acceptable given that the air flow rate and temperature of the Fuel Cell are linked to its efficiency and health. The black dashed line shows the temperature output from the Sliding Mode controller. Compared to the P and PI the SMC has a much lower settling time (around 70 seconds) and thus is able to reach the desired stack temperature much faster. As an example it can be seen that both P and PI controllers are unable to bring down the FC temperature quickly between 600 to 800 second period while the SMC reduces the temperature with least delay. The SMC is more robust to handle the abrupt load changes and settle quickly on an optimum temperature for that particular current. It can be argued that the SMC allows a faster rise in temperature compared to P and PI for increasing loads. However reaching the optimum temperature quickly regardless of rising or falling current is very important. The best performance is gained at the optimum temperatues and any delays in achieving these temperatures will add to inefficiencies.

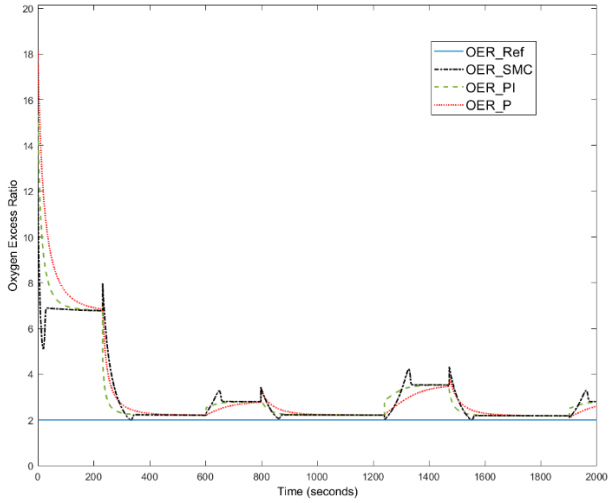

Fig. 15 OER of the PEMFC as a result of the three different controllers.

Fig. 15 represents the OER output from all 3 controllers . The solid blue line gives the reference OER at 2. At low current interval, the OER is high and drops to lower values when the current demand is increased. It must be noted that the fans supplying the oxygen in the FC have a lower RPM limit which means that the flowrate cannot drop proportionally for very low currents. For this case, a lower flowrate limit was set to get a more realistic result. Since the fan starts with its own minimum flow rate and this may be much larger than required at the low current – initial spikes can be seen in the OER plots. The OER is well maintained above 2 due to the fact that the reference temperature is derived from the OER requirements as well as the cooling requirements. The SMC controller results are shown in a black dashed line. While all control schemes were able to maintain an OER above 2, the SMC controller had a much faster settling time making it the controller of choice from those compared in this study. The multiple peaks during load changes show how quickly and closely the SMC controller is able to change its output with change in load. The SMC controller is robust enough to utilize the simplified model to achieve the desired control objectives. The results also point at the importance of considering both the temperature and OER together in the control scheme.

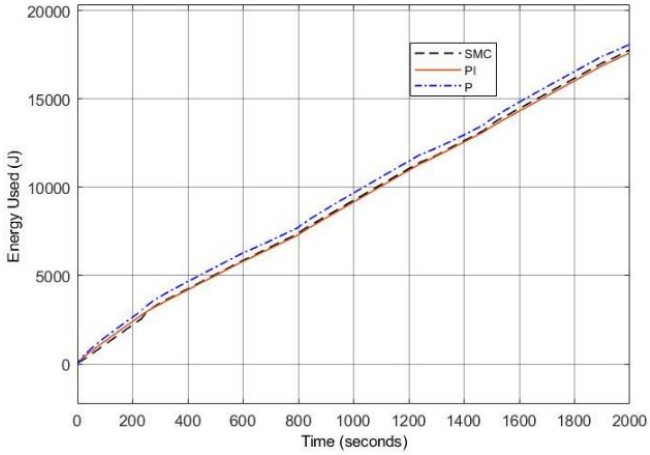

Fig. 16 Energy used in different controller scenarios

Fig. 16 shows how much energy is used by the fans in each controller scenario for the entire simulation period. The flowrate in the system was modelled based on 2 of 15 W fans and based on the different responses the consumption of energy was different for different controllers. The proportional (P) controller expands the most energy to achieve the cooling. The SMC uses slightly more energy than the PI control scheme but as explained in the results section the SMC is a much faster controller.

The disadvantage of the slower controller is that the optimum temperature and OER is not reached quickly and the health of the PEMFC system suffers. The advantage is that the slow responding PI controller allows less energy to be used. However, the energy saved is very less compared to the rated power of the fuel cell in this case (PEMFC is rated at 1.2 kW). Even if the fans are running at 100% all the time – they can only use 2.5% of the rated power of the PEMFC. While the PI controller does save some minor amount of energy and reduces the parasitic load – in the long run the durability of the PEMFC is compromised. Hence it is the SMC control scheme which is better than the P and PI schemes.

The P and PI control schemes are linear control schemes while the SMC is a nonlinear control scheme. This allows the SMC to consider the nonlinear behaviors in the system and thus the responses are more accurate. Fuel Cells, just like most real-life systems are nonlinear and as such the approximations in a traditional linear control scheme may not offer accurate responses and need more settling time to reach the setpoints. The SMC is also better able to handle abrupt current changes which are essentially disturbances to the system. The step load profile is much better handled by the SMC due to this robustness. The addition of the excess ratio in setting refence temperature allows all controllers to maintain an OER above 2 but the SMC appears to be the fastest and most robust. Apart from the comparison of the controllers, the comparison is also made between different control objectives and how that affects the FC in terms of performance. Thermal and air management in Open Cathode PEMFC systems are extremely critical and need to be treated together for optimum performance.

V. CONCLUSION

The paper presents a simplified nonlinear dynamic model which uses just four state variables to model the changes in an Open Cathode PEMFC system under a step load profile. Results show that with accurate parameter estimations, the model is in agreement with measured results from the 1.2kW PEMFC. Three different control topologies are applied to the simplified model in order to control the temperature and OER in the PEMFC. The topologies of PI and SMC were applied in direct OER control while P, PI and SMC were applied to control the stack temperature directly. It was seen that while controlling just the OER or just the temperature – the optimum conditions are not reached. The results showed chances of permanent degradation of the PEMFC. The authors thus employed a third scheme of using the OER to determine a new reference temperature in a temperature control scheme. This produced the most favorable results and maintained the OER as well as the system temperature at desired levels. The SMC scheme had the fastest response and settled at the setpoint within around 70 seconds while the Proportion control scheme was the slowest – having delays in the order of 200- 250 seconds. Given the SMC is well suited to nonlinear systems, the results of the SMC were superior to the linear control schemes of P and PI. However, the SMC controller was found to have the more parasitic energy losses due to its fast response in achieving the reference temperature. While the parasitic losses are an important consideration, in this case the energy losses due to the SMC controller over other controllers is a very small portion of the rated power of the PEMFC system. The SMC controller expands slightly more energy through the fans but improves the response of the PEMFC and increases the life of the PEMFC by reducing degradation caused by low OER and undesirable temperatures.

REFERENCES

[1] "Fuel Cells: Principles, Types, Fuels, and Applications - Carrette - 2000 - ChemPhysChem - Wiley Online Library." https://chemistry-europe.onlinelibrary.wiley.com/doi/10.1002/1439-7641%2820001215%291%3A4%3C162%3A%3AAID-CPHC162%3E3.0.CO%3B2-Z (accessed Feb. 18, 2022).

[2] S. Laghrouche, I. Matraji, F. S. Ahmed, S. Jemei, and M. Wack, “Load governor based on constrained extremum seeking for PEM fuel cell oxygen starvation and compressor surge protection,” *International Journal of Hydrogen Energy*, vol. 38, no. 33, pp. 14314–14322, Nov. 2013, doi: 10.1016/j.ijhydene.2013.08.109.
[3] A. Mohammadi, A. Djerdir, N. Yousfi Steiner, and D. Khaburi, “Advanced diagnosis based on temperature and current density distributions in a single PEMFC,” *International Journal of Hydrogen Energy*, vol. 40, no. 45, Art. no. 45, Dec. 2015, doi: 10.1016/j.ijhydene.2015.04.157.
[4] A. Mohammadi, D. Chabane, G. Cirrincione, M. Cirrincione, and A. Djerdir, “Effect of the Temperature Distribution on the Performance of PEMFC Stacks for Fault Diagnosis,” in *2018 21st International Conference on Electrical Machines and Systems (ICEMS)*, Oct. 2018, pp. 1019–1023. doi: 10.23919/ICEMS.2018.8549518.
[5] O. S. Ijaodola, Z. El- Hassan, E. Ogungbemi, F. N. Khatib, T. Wilberforce, J. Thompson, and A. G. Olabi, “Energy efficiency improvements by investigating the water flooding management on proton exchange membrane fuel cell (PEMFC),” *Energy*, vol. 179, pp. 246–267, Jul. 2019, doi: 10.1016/j.energy.2019.04.074.
[6] W.-W. Yuan, K. Ou, and Y.-B. Kim, “Thermal management for an air coolant system of a proton exchange membrane fuel cell using heat distribution optimization,” *Applied Thermal Engineering*, vol. 167, p. 114715, Feb. 2020, doi: 10.1016/j.applthermaleng.2019.114715.
[7] J. T. Pukrushpan, A. G. Stefanopoulou, and H. Peng, “Modeling and control for PEM fuel cell stack system,” in *Proceedings of the 2002 American Control Conference (IEEE Cat. No.CH37301)*, May 2002, pp. 3117–3122 vol.4. doi: 10.1109/ACC.2002.1025268.
[8] L.-Y. Chiu and B. M. Diong, “An improved small-signal model of the dynamic behavior of PEM fuel cells,” in *38th IAS Annual Meeting on Conference Record of the Industry Applications Conference, 2003.*, Oct. 2003, pp. 709–715 vol.2. doi: 10.1109/IAS.2003.1257597.
[9] G. Marsala, M. Pucci, G. Vitale, M. Cirrincione, and A. Miraoui, “A prototype of a fuel cell PEM emulator based on a buck converter,” *Applied Energy*, vol. 86, no. 10, pp. 2192–2203, Oct. 2009, doi: 10.1016/j.apenergy.2008.12.028.
[10] J. Chen, Z. Liu, F. Wang, Q. Ouyang, and H. Su, “Optimal Oxygen Excess Ratio Control for PEM Fuel Cells,” *IEEE Transactions on Control Systems Technology*, vol. 26, no. 5, pp. 1711–1721, Sep. 2018, doi: 10.1109/TCST.2017.2723343.
[11] M. A. Danzer, J. Wilhelm, H. Aschemann, and E. P. Hofer, “Model-based control of cathode pressure and oxygen excess ratio of a PEM fuel cell system,” *Journal of Power Sources*, vol. 176, pp. 515–522, Jan. 2008, doi: 10.1016/j.jpowsour.2007.08.049.
[12] W. R. W. Daud, R. E. Rosli, E. H. Majlan, S. A. A. Hamid, R. Mohamed, and T. Husaini, “PEM fuel cell system control: A review,” *Renewable Energy*, vol. 113, pp. 620–638, Dec. 2017, doi: 10.1016/j.renene.2017.06.027.
[13] J. Zhang, Y.-X. Wang, H. He, and Y. Wang, “Active Thermal Management for an Automotive Water-Cooled Proton Exchange Membrane Fuel Cell by Using Feedback Control,” in *2020 IEEE Vehicle Power and Propulsion Conference (VPPC)*, Nov. 2020, pp. 1–5. doi: 10.1109/VPPC49601.2020.9330959.
[14] C. H. Woo and J. B. Benziger, “PEM fuel cell current regulation by fuel feed control,” *Chemical Engineering Science*, vol. 62, no. 4, pp. 957–968, Feb. 2007, doi: 10.1016/j.ces.2006.10.027.
[15] M. Serra, J. Aguado, X. Ansede, and J. Riera, “Controllability analysis of decentralised linear controllers for polymeric fuel cells,” *Journal of Power Sources*, vol. 151, pp. 93–102, Oct. 2005, doi: 10.1016/j.jpowsour.2005.02.050.
[16] S. N. Giménez, J. M. H. Durá, F. X. B. Ferragud, and R. S. Fernández, “Design and Experimental Validation of the Temperature Control of a PEMFC Stack by Applying Multiobjective Optimization,” *IEEE Access*, vol. 8, pp. 183324–183343, 2020, doi: 10.1109/ACCESS.2020.3029321.
[17] W.-J. Zou and Y.-B. Kim, “Temperature Control for a 5 kW Water-Cooled PEM Fuel Cell System for a Household Application,” *IEEE Access*, vol. 7, pp. 144826–144835, 2019, doi: 10.1109/ACCESS.2019.2945986.
[18] D. Zhao, F. Li, R. Ma, G. Zhao, and Y. Huangfu, “An Unknown Input Nonlinear Observer Based Fractional Order PID Control of Fuel Cell Air Supply System,” *IEEE Transactions on Industry Applications*, vol. 56, no. 5, pp. 5523–5532, Sep. 2020, doi: 10.1109/TIA.2020.2999037.
[19] Q. Chen, J. Chen, and Y.-X. Wang, “Open Cathode Type of Fuel Cell Stack Temperature Regulation by Active Disturbance Rejection Control,” in *2020 Chinese Automation Congress (CAC)*, Nov. 2020, pp. 3435–3440. doi: 10.1109/CAC51589.2020.9326870.
[20] M. Gheisarnejad, J. Boudjadar, and M.-H. Khooban, “A New Adaptive Type-II Fuzzy-Based Deep Reinforcement Learning Control: Fuel Cell Air-Feed Sensors Control,” *IEEE Sensors Journal*, vol. 19, no. 20, pp. 9081–9089, Oct. 2019, doi: 10.1109/JSEN.2019.2924726.
[21] Y. Shtessel, C. Edwards, L. Fridman, and A. Levant, *Sliding mode control and observation*, vol. 10. Springer, 2014.
[22] V. Utkin, “Variable structure systems with sliding modes,” *IEEE Transactions on Automatic Control*, vol. 22, no. 2, pp. 212–222, Apr. 1977, doi: 10.1109/TAC.1977.1101446.
[23] L. Wu, J. Liu, S. Vazquez, and S. K. Mazumder, “Sliding Mode Control in Power Converters and Drives: A Review,” *IEEE/CAA Journal of Automatica Sinica*, vol. 9, no. 3, Art. no. 3, Mar. 2022, doi: 10.1109/JAS.2021.1004380.
[24] C.-T. Chen and S.-T. Peng, “A sliding mode control scheme for non-minimum phase non-linear uncertain input-delay chemical processes,” *Journal of Process Control*, vol. 16, no. 1, pp. 37–51, Jan. 2006, doi: 10.1016/j.jprocont.2005.04.009.
[25] J. Liu, Y. Gao, X. Su, M. Wack, and L. Wu, “Disturbance-Observer-Based Control for Air Management of PEM Fuel Cell Systems via Sliding Mode Technique,” *IEEE Transactions on Control Systems Technology*, vol. 27, no. 3, pp. 1129–1138, May 2019, doi: 10.1109/TCST.2018.2802467.
[26] K. Sankar and A. K. Jana, “Nonlinear multivariable sliding mode control of a reversible PEM fuel cell integrated system,” *Energy Conversion and Management*, vol. 171, pp. 541–565, Sep. 2018, doi: 10.1016/j.enconman.2018.05.079.
[27] S. S. Kumar, M. Cirrincione, V. Léchappé, K. R. Ram, and A. Mohammadi, “A Simplified Control Oriented Model Of an Open Cathode PEM Fuel Cell,” in *2021 IEEE 12th Energy Conversion Congress Exposition - Asia (ECCE-Asia)*, May 2021, pp. 2415–2420. doi: 10.1109/ECCE-Asia49820.2021.9479098.
[28] C. Spiegel, *PEM fuel cell modeling and simulation using MATLAB*. Elsevier, 2011.
[29] L. Khotseng, “Fuel Cell Thermodynamics,” in *Thermodynamics and Energy Engineering*, P. Vizureanu, Ed., IntechOpen, 2020. doi: 10.5772/intechopen.90141.
[30] R. O’Hayre, S.-W. Cha, W. Colella, and F. B. Prinz, *Fuel Cell Fundamentals*. John Wiley & Sons, 2016.
[31] J. C. Amphlett, R. M. Baumert, R. F. Mann, B. A. Peppley, P. R. Roberge, and T. J. Harris, “Performance Modeling of the Ballard Mark IV Solid Polymer Electrolyte Fuel Cell: I . Mechanistic Model Development,” *J. Electrochem. Soc.*, vol. 142, no. 1, p. 1, Jan. 1995, doi: 10.1149/1.2043866.
[32] K. R. Ram, K. Naidu, R. Kumar, M. Cirrincione, and A. Mohammadi, “Model Comparison and Parameter Estimation of Polymer Exchange Membrane (PEM) Fuel Cell Based on Nonlinear Least Squares Method,” in *2019 International Aegean Conference on Electrical Machines and Power Electronics (ACEMP) 2019 International Conference on Optimization of Electrical and Electronic Equipment (OPTIM)*, Aug. 2019, pp. 500–505. doi: 10.1109/ACEMP-OPTIM44294.2019.9007136.
[33] K. Ou, W.-W. Yuan, M. Choi, S. Yang, and Y.-B. Kim, “Performance increase for an open-cathode PEM fuel cell with humidity and temperature control,” *International Journal of Hydrogen Energy*, vol. 42, no. 50, pp. 29852–29862, Dec. 2017, doi: 10.1016/j.ijhydene.2017.10.087.
[34] Q. Jian, B. Huang, L. Luo, J. Zhao, S. Cao, and Z. Huang, “Experimental investigation of the thermal response of open-cathode proton exchange membrane fuel cell stack,” *International Journal of Hydrogen Energy*, vol. 43, no. 29, pp. 13489–13500, Jul. 2018, doi: 10.1016/j.ijhydene.2018.05.097.